


RESEARCH ARTICLE

Demyelination in hereditary sensory neuropathy type-1C

Sadaf Saba^{1,a} , Yongsheng Chen^{2,a}, Krishna Rao Maddipati³, Melody Hackett², Bo Hu² & Jun Li^{1,2,4,5}

¹Center for Molecular Medicine and Genetics, Wayne State University School of Medicine, Detroit, Michigan

²Department of Neurology, Wayne State University School of Medicine, Detroit, Michigan

³Lipidomics Core Facility, Department of Pathology, Wayne State University School of Medicine, Detroit, Michigan

⁴Department of Biochemistry, Microbiology and Immunology, Wayne State University School of Medicine, Detroit, Michigan

⁵John D. Dingell VA Medical Center, Detroit, Michigan

Correspondence

Jun Li, Department of Neurology, Wayne State University School of Medicine, 4201 St. Antoine, UHC8D, Detroit, MI 48201.
Tel: 313-577-8824; Fax: 313-745-4216;
E-mail: junli@med.wayne.edu

Funding Information

This study is supported by grants from NIH (R01NS066927), VA BLR&D (IBX003385A), and Detroit Medical Center Foundation (2018-3328).

Received: 21 May 2020; Revised: 21 May 2020; Accepted: 30 May 2020

Annals of Clinical and Translational Neurology 2020; 7(9): 1502–1512

doi: 10.1002/acn3.51110

^aThese two authors contributed equally.

Introduction

Hereditary sensory and autonomic neuropathy type 1 (HSAN1) is a slowly progressive dominantly inherited polyneuropathy with variable sensory and motor deficits. It has also been called hereditary sensory neuropathy (HSN1) due to negligible autonomic involvements in many patients with the disease. Upon physical examination, patients may show distal muscle weakness, atrophy, depressed deep tendon reflexes and altered pain/temperature perception.^{1,2} Axonal loss involving all different diameters of nerve fibers has been reported in sural nerve and skin biopsies from patients with HSN1.^{1,3}

Sphingolipids (SLs) are bioactive molecules with critical roles in neural cells.⁴ They incorporate into the cell

Abstract

Objective: Sphingolipids are enriched in the nerves. Serine-palmitoyltransferase (SPT) catalyzes the key step of sphingolipids biosynthesis. Mutations in SPT subunits (SPTLC) lead to the excessive production of neurotoxic deoxysphingolipids (DoxSLs) in patients with Hereditary Sensory Neuropathy Type-1C (HSN1C). HSN1C is an autosomal dominant peripheral neuropathy characterized by sensory loss and distal muscle weakness. In this study, by leveraging a HSN1C family with a previously reported N177D mutation in *SPTLC2*, we aim to further define the spectrum of DoxSL species and the peripheral nerve pathology of the disease. **Methods:** Next-generation sequencing along with Sanger confirmation was performed for family members and healthy controls. LC-MS was used for lipidomic analysis in participants' plasma. Quantitative magnetic resonance imaging (qMRI) was performed to study sciatic nerve pathologies. **Results:** A heterozygous N177D mutation in *SPTLC2* was co-segregated in individuals with sensory-motor deficits in the limbs. Nerve conduction studies (NCS) revealed nonuniform slowing of conduction velocities. In line with the NCS, qMRI detected a pattern of nerve changes similar to those in acquired demyelinating polyneuropathies. Additionally, we detected a significant increase in multiple species of deoxysphingoid bases and deoxyceramides in patients' plasma. **Interpretation:** Mutations in the *SPTLC2* cause a demyelinating phenotype resembling those in acquired demyelinating polyneuropathy. The species of increased DoxSLs in HSN1C may be more diverse than originally thought.

membranes⁵ and modulate the biophysical properties of myelin, thereby affecting action potential propagation. Mutations in enzymes involved in SL metabolism have been linked to neurodegenerative diseases, which highlight the importance of SLs in neural functions.⁴ The serine-palmitoyltransferase (SPT) enzyme is a heterodimeric protein, consisting of SPT long chain base unit (SPTLC1) complexed with SPTLC2 or SPTLC3. It catalyzes the first step of SL biosynthesis by condensing L-serine to palmitoyl-CoA (Fig. 1).⁴ Early products of this pathway, free sphingoid bases including sphingosine (SO) and sphinganine (SA), are known to interact with specific receptors and activate numerous biological processes. Ceramides and dihydroceramides are produced later by acylation of these sphingoid bases.⁶ Under normal conditions,

deoxysphingoid bases (DoxSBs), deoxyceramides (DoxCer) and 1-deoxydihydroceramides (DoxDHCer) are at very low levels.⁵ However, elevation of different SL metabolites and DoxSLs have been shown in pathological conditions including HSN1, diabetes, autoimmune diseases, and various inflammatory and neurodegenerative disorders.^{5,7,8}

Missense mutations in *SPT long chain base subunit 1 or 2* (*SPTLC 1 or 2*) may reduce enzymatic activity and shift substrate specificity from L-serine to L-alanine and glycine, which generates excessive DoxSBs, including 1-deoxysphinganine (DoxSA), 1-deoxysphingosine (DoxSO), and 1-deoxymethylsphinganine (DoxmethSA)^{4,9} (Fig. 1). In heterozygous *Sptlc1* and two knock-out mice,¹⁰ yeasts with missense mutations of these genes¹¹ and transgenic mouse models overexpressing the mutant gene,¹² enzymatic activity of SPT was reduced. A change

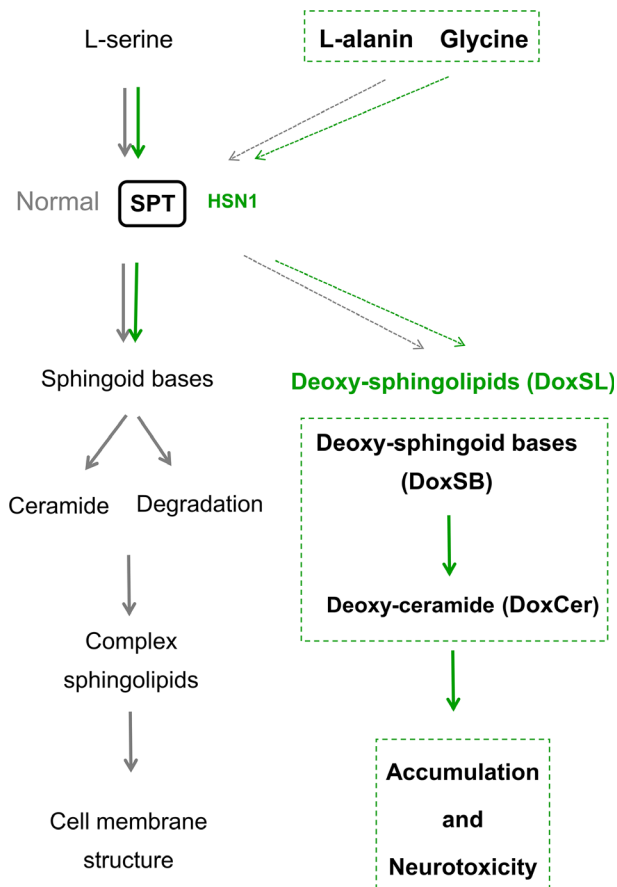


Figure 1. Illustration of the synthetic pathway of sphingolipids. Sphingoid bases (i.e SA) and ceramides are produced from L-serine catalyzed by the Serine palmitoyl transferase (SPT) enzyme. When SPT is mutated, such as in HSN1, deoxy-sphingoid bases (DoxSBs) are produced due to the altered SPT specificity toward L-alanine and Glycine. Additional species of Deoxy-ceramides (DoxCers) can be derived from those DoxSBs that accumulate and cause neurotoxicity.

in substrate selectivity of the SPT by missense mutations in *SPTLC1* has also been confirmed in transgenic mice, suggesting a gain-of-function nature of the HSN1 mutations.¹³ These mutations in *SPTLC* are relevant to the pathogenesis in HSN1⁹ because DoxSBs have been shown to impair axonal structure.^{4,9} DoxSBs and the derived DoxCers resulting from these mutations have been shown to disturb synaptic growth at neuromuscular junctions in drosophila¹⁴ and axonal vesicular trafficking in *Caenorhabditis elegans*.¹⁵ Interestingly, correction of DoxSB levels reversed the nerve pathology in a HSN1 animal model and the diabetic animal model.^{16,17} However, it is yet to be determined if additional DoxSL species are altered in patients with HSN1.⁴ Given that the degree of cytotoxicity from different DoxSLs varies, our knowledge of the full spectrum of DoxSLs is important for understanding the pathogenesis of the disease.^{16,17}

We have identified a family with HSN1C where a demyelinating polyneuropathy was found. This phenotype is in line with the abundance of sphingolipids in myelin and raises the question of how DoxSLs (DoxSBs + DoxCers) might affect myelin in the peripheral nerves. Distal nerves in HSN1C are often severely degenerated leading to nonresponsiveness in nerve conduction studies (NCS). Therefore, we targeted proximal nerves using quantitative magnetic resonance imaging (qMRI), which provided helpful information about the myelin.

Subjects and Methods

Patients

Six patients and three nonaffected members from the proband's family (Fig. 2) were evaluated in our Charcot-Marie-Tooth (CMT) clinic at Detroit Medical Center, Wayne State University. Four normal controls (age and sex matched) outside of this family were enrolled for lipidomic studies. This study was approved by the institutional review board at the Wayne State University. Written consent was obtained from all participants.

In addition to medical history and neurological examination, a CMT neuropathy score (CMTNS) was obtained from all patients to measure clinical impairments.¹⁸ The score is comprised of sensorimotor symptoms, physical findings in limbs and nerve conduction studies. CMTNS ranges from 0 to 36, with 36 being the most severely affected.

Nerve conduction studies (NCS)

NCS were performed as previously described.¹⁹ The distal stimulation distance for motor nerves in the arms and

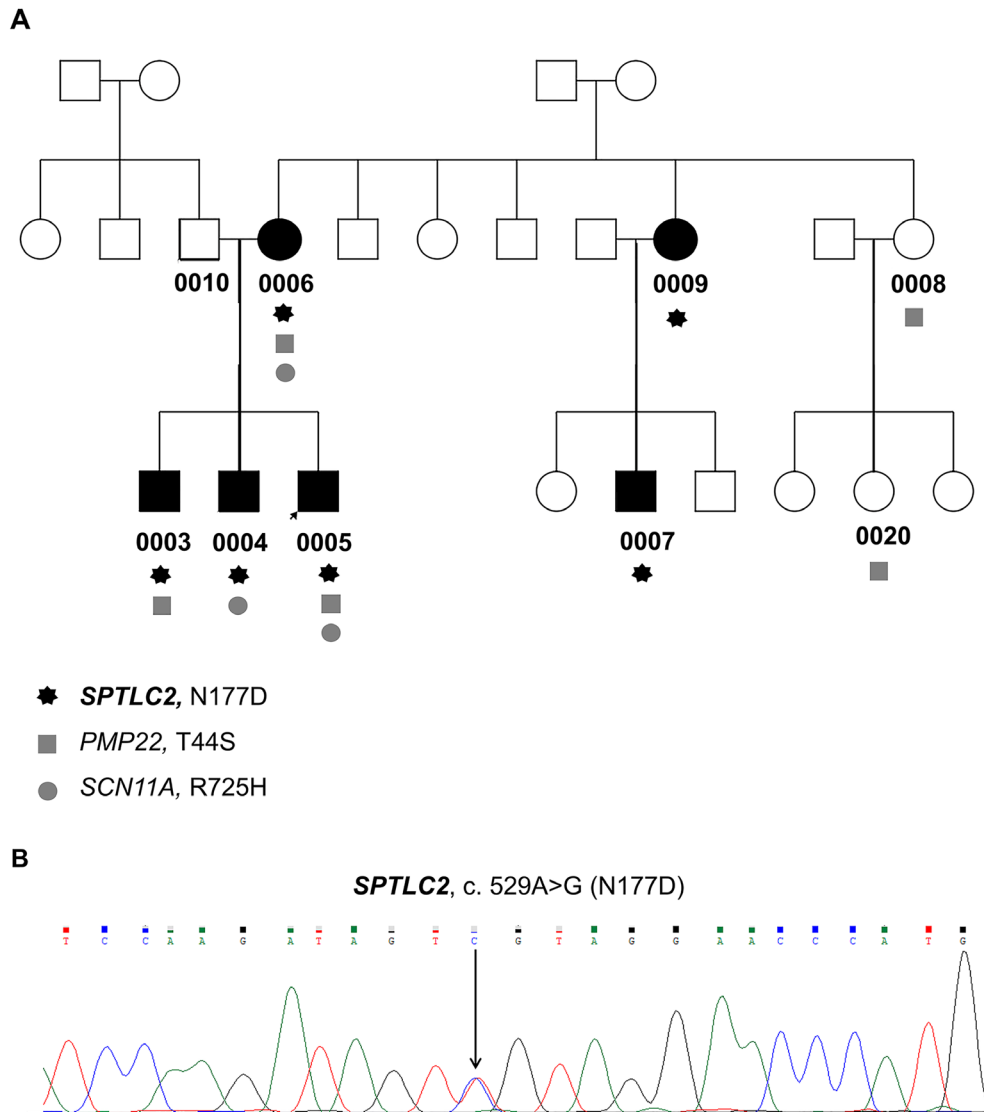


Figure 2. Pedigree of the studied family and their Sanger sequencing results. (A) Subject with an arrow is the proband that was examined initially in clinic. Other subjects marked with numerical codes were enrolled into the study subsequently. Male-to-male transmission supports an autosomal dominant inheritance. (B) Sanger sequencing showed a heterozygous mutation (c. 529A > G, p. N177D; arrow) in *SPTLC2* in all affected subjects, but not in others.

legs was 7 and 9 cm, respectively. The stimulation distance for the sensory nerves in median, ulnar, and sural nerves was 14 cm, but for the radial nerve it was 11 cm.

DNA sequencing

DNA of the proband (#0005) was evaluated by a targeted gene panel (72 CMT-related genes) using next-generation sequencing in Invitae (San Francisco, CA). Participants (#0003 and #0004) were Sanger-sequenced for three genes (*PMP22*, *SCN11A* and *SPTLC2*) through Invitae. Enrichment of the targeted regions was done using a

hybridization-based protocol and sequencing was performed on the Illumina HiSeq 2500 platform with >50× read depth, and >99% sensitivity/specificity for single-nucleotide variants. Furthermore, specific missense variants in *PMP22*, *SCN11A*, and *SPTLC2* were verified by Sanger sequencing in our laboratory for the rest of participants. DNA for the Sanger sequencing was extracted from blood cells using a commercial kit (#A1620; Promega, Madison, WI). The sequencing was performed at Genewiz Corporation (South Plainfield, NJ, USA). The sequences were analyzed using Chromas (V 2.6.6; Technelysium Pty Ltd, South Brisbane, Australia).

Lipidomic analysis

Blood was drawn into an EDTA vacutainer and centrifuged at 2000g for 10 min at room temperature. The upper plasma was aspirated into a tube and stored at -80°C . Sphingolipids were extracted with isopropanol-ethyl acetate (3:7).²⁰ Sphingoid bases and their phosphates were analyzed by MRM methods following HPLC separation on C8 columns.²¹

For sphingolipidomic analyses, high-performance liquid chromatography (HPLC) was performed on a Prominence XR system (Shimadzu) using a Targa C8 column (5 μ , 2.1 \times 20 mm, Higgins Analytical). The mobile phase consists of a gradient between A: methanol-water-ammonium formate-formic acid (5:95:1 mmol/L:0.2 v/v) and B: methanol-ammonium formate-formic acid (100:2 mmol/L:0.2 v/v). The composition of B was as follows: 0 min, 35%; 2 min, 100%; and 5 min, 100%. The flow rate was 0.5 mL/min. The HPLC eluate was directly introduced to the ESI source of the QTRAP5500 mass analyzer (ABSCIEX) in the positive ion mode with the following conditions: Curtain gas: 35 psi, GS1: 45 psi, GS2: 45 psi; Temperature: 650°C ; Ion Spray Voltage: 5500 V; Collision gas: low; Declustering Potential: 100 V; Entrance Potential: 10 V. The eluate was monitored by the Multiple Reaction Monitoring method to detect unique molecular ion–daughter ion combinations for each of the sphingolipids and long chain bases (sphingosines) with 100-msec dwell time for each transition. Optimized Collisional Energies (16 to 28 eV) and Collision Cell Exit Potentials (10 V) were used for each MRM transition. The samples were analyzed for ceramides and sphingomyelins using precursor ion scans, m/z 264 and 184. The data were acquired using Analyst 1.6.2 and the MRM transition chromatograms were quantitated by MultiQuant (from ABSCIEX). Internal standards for ceramides were Cer (d18:1/17:0). Internal standards used for deoxysphingoid bases and deoxymethylsphingoid bases were 1-Deoxysphinganine-d3 (m18:0-d3) and 1-deoxymethylsphinganine-d7 (m17:0-d7, respectively). The internal standards were used to normalize recovery as well as relative quantitation of each analyte.

Quantitative magnetic resonance imaging (qMRI)

All subjects were scanned on a 3T system (Verio, Siemens Healthineers, Erlangen, Germany) with an 8-channel knee coil positioned proximal to the knee. An established imaging protocol was performed in the axial plane.²² It includes: (1) an interleaved two-point Dixon three dimensional (3D) gradient recalled echo (GRE) scan for muscle fat fraction (FF)^{23,24}; (2) a high-resolution 3D

GRE scan for nerve fascicle cross-sectional area (fCSA); (3) a dual-echo two dimensional (2D) turbo spin echo (TSE) scan for nerve transverse relaxation rate (R2) measure; (4) the strategically acquired gradient echo (STAGE) imaging²⁵ for nerve longitudinal relaxation time (T1), proton density (PD) and effective transverse relaxation rate (R2*) measurements, which generated the radiofrequency (RF) field maps (B_1^+ and B_1^-) simultaneously for correcting RF variations in the T1, PD, and magnetization transfer ratio (MTR) maps; (5) two 3D GRE scans performed with and without MT pulses for nerve MTR; and (6) a diffusion tensor imaging (DTI) scan for nerve apparent diffusion coefficient (ADC) and fractional anisotropy (FA).

An in-house developed program in MATLAB (R2019a, MathWorks, Natick, MA, USA) was used to process the qMRI results. All images were co-registered using SPM (fil.ion.ucl.ac.uk/spm/) prior to the processing pipeline.

For muscle qMRI, a pixelwise fat fraction (FF) image was given by $\text{FF} = F/(W + F) \times 100\%$, where F is the fat image and W is the water (muscle) image generated from the two-point Dixon algorithm.²⁴ Whole-muscle mean fat fraction (wmmFF) was measured on the FF image using an established semi-automated segmentation to delineate muscular boundaries on the central slice of the water image.²²

For nerve qMRI, the R2 map was calculated to be $R2 = \ln(I_{TE1}/I_{TE2})/(TE_2 - TE_1)$, where $I_{TE1,TE2}$ and $TE_{1,2}$ are the pixel intensities and echo times of the two echoes from the dual-echo TSE scan. A simple linear regression calculation was used to generate the R2* map on the two echoes of STAGE scan. To extract T1, PD, B_1^+ , B_1^- maps, STAGE algorithm²⁵ was performed using two reference regions: subcutaneous fat ($T1_{\text{fat}} = 370$ msec) and muscle ($T1_{\text{muscle}} = 1400$ msec).²⁶ The MTR was calculated to be $\text{MTR} = (S_0 - S_{\text{MT}})/S_0 \times 100\%$, where S_0 and S_{MT} are the signal intensities acquired without and with MT. The ADC and FA were reconstructed directly from the scanner though the DTI scan. Similar to the muscle segmentation, a sciatic nerve fascicular binary mask (1 for nerve fascicle pixels and 0 for other pixels) was delineated on the central slice of high-resolution 3D GRE scan to measure nerve fCSA. The nerve fascicular mask was then used on other qMRI images to extract T1, PD, R2, R2*, MTR, ADC, and FA for nerves.

Statistics

Comparison of continuous variables between two groups was done through a Student's t -test (unpaired, two tailed) using MATLAB with in-house developed scripts. The age and BMI were also compared between the two groups using the same t -test. A threshold of $P < 0.05$ was considered to be statistically significant.

Results

Clinical presentation

Case presentation

Patient #0005: The proband is a 36-year-old man who had a normal development until he started to trip and fall at 24 years of age. This was associated with pain in his shins, fatigue and weakness in his legs. He experienced numbness and tingling one year after the onset of weakness. He began to wear ankle braces around 27 years of age. By the time of his clinic visit, he reported no sensation in his feet. In his early 30s, he experienced numbness in the fingertips, followed by loss of sensation, weakness, and muscle cramps in his hands.

On neurological examination, he had pes cavus and muscle atrophy in the feet and legs. He was an information technologist (IT); and showed normal mental status and cranial nerve functions. Muscle strength was a 2 on the MRC scale in ankle dorsal flexors, 4 in hand intrinsic muscles, but 5 in other muscles. Sensation to pin prick was absent in his hands and legs below the knees. Sensation to vibration was absent in toes and decreased at ankles, fingers and wrists. Deep tendon reflexes were absent in ankles and knees.

Clinical phenotype in other family members

Two brothers (#0003 and #0004) of the proband had normal development and excelled in sports until high school. They became symptomatic around their 20s with symptoms similar to the proband. None reported syncope, changes in perspiring or erectile function.

While similar symptoms were found in their mother, aunt, and cousin, the phenotype was milder with later onset. The differences were reflected by CMTNS ranging from 17 (moderate) to 27 (severe) in the three brothers; but lower in their mother (#0006, score 4) and cousin (#0007, score 11) (Table 1).

Table 1. Clinical features in patients with HSN1C.

Code	0003	0004	0005	0006	0007	0009
Sex/age	M/33	M/27	M/36	F/63	M/41	F/67
Sensory loss	Y	Y	Y	Y	Y	Y
Pain	N	N	Y	Y	N	N
Ankle weakness	Y	Y	Y	N	Y	N
Thigh muscle weakness	N	N	N	N	N	N
Hand muscle weakness	Y	Y	Y	N	N	N
Foot deformity	N	N	Y	N	N	N
CMTNS	24	17	27	4	11	NA

Y, Yes; N, No; NA, Not available.

Electrophysiological manifestation

NCS was done on the six affected members of the family (Table 2) and showed sensorimotor polyneuropathy with slowed conduction velocity (CV). CVs were nonuniform. For instance, the ulnar motor nerve CV was 68 m/sec in #0006, but only 27 m/sec in the tibial motor nerve of the same patient. The peroneal motor nerve CV was 38 m/sec, but only 25 m/sec in the tibial motor nerve of #0009. The findings are suggestive of segmental demyelination.^{27,28} Nerves in the legs were often nonresponsive, suggesting secondary axonal loss.

Genotypic findings

DNA analysis of the proband (#0005) revealed three heterozygous variants in *PMP22* (T44S with rs112651887, five alleles in gnomAD, MAF = 0.00001988), *SCN11A* (R725H with rs752954989, six alleles in gnomAD, MAF = 0.00002124), and *SPTLC2* (N177D with rs1131691917). Sanger sequencing in all family members demonstrated that only the N177D mutation in *SPTLC2* was co-segregated with affected family members (Fig. 2A).

The missense variant (c. 529A > G) on exon 4 of *SPTLC2* leads to the replacement of a highly conserved asparagine with an aspartic acid at codon 177 (p. Asn177Asp or N177D). In *Silico* analysis predicted that N177D is “Deleterious” and “Probably damaging” by SIFT and Polyphen, but GVGID identified it as “less likely interfering with protein function”. This variant was absent in databases such as gnomAD and the Inherited Neuropathy Variant Browser (INVB).²⁹ There are three entries of the N177D variant in ClinVar showing co-segregation with the HSN1 phenotype in families. A recent publication reported the N177D mutation also segregating in another HSN1C family.³⁰ Collectively, these observations support the pathogenic effect of the N177D mutation in *SPTLC2*.

Plasma lipid analysis

All affected family members carrying the N177D mutation showed a significant increase in DoxSBs compared to healthy controls (age/gender matched; Fig. 3A): 1-deoxysphinganine (DoxSA) (0.66 ± 0.27 vs. $0.17 \pm 0.08 \mu\text{mol/L}$; $P < 0.001$), and 1-deoxysphingosine (DoxSO) (1.28 ± 0.27 vs. $0.44 \pm 0.17 \mu\text{mol/L}$; $P < 0.001$). In addition, DoxCers that are downstream products to DoxSBs were increased; examples: Cer(m18:0/16:0), Cer(m18:1/18:0) and Cer(m18:0/18:0) derived from L-alanine and Cer(m17:0/24:0) and Cer(m17:1/24:0) from glycine (Fig. 3B). Of these species, Cer(m18:0/16:0)

Table 2. Electrophysiological findings of the studied family members.

Code #	Sensory nerve conduction, DL/Amp/CV				Motor nerve conduction, DL/Amp/CV			
	Median	Ulnar	Radial	Sural	Median	Ulnar	Peroneal	Tibial
Norm	3.5/22/50	3.5/10/50	2.7/10/48	4.4/6.0/40	4.4/4.0/49	3.3/6.0/49	6.5/2.0/44	2.0/6.1/40
0003	NR	7/6.4/25.6	3.3/0.7/40	NR	5.5/0.3/26.6	3.4/2.5/47	NR	NR
0004	NR	7/1.5/25.4	NR	NR	4.7/0.5/30.9	3.8/4.3/32.7	NR	NR
0005	NR	6.1/1.5/29.5	NR	NR	NR	4.4/0.7/30.5	NR	NR
0006	3.7/17.5/49	3.1/19.8/57	2.1/45.3/62	4.8/7.4/39	3.8/7.4/62	2.2/12.3/68	NA	4.4/3.9/27
0007	10.3/7.5/17	4.6/4.4/36	7.1/17.3/19	3.9/4.4/49	4.1/5.0/38	3.4/4.4/52	NR	NR
0009	NA	NA	NA	NA	NA	NA	4.17/1.6/38	5.2/1.6/25

DL/Amp/CV, Distal Latency/Amplitude/Conduction Velocity; Norm, Normative values; NR, Not Responsive; NA, Not Available; NCS was not done on patient's arm/leg.

(24 ± 14 nmol/L vs. 5.5 ± 1.8 nmol/L; $P < 0.05$) and Cer(m18:1/18:0) (69.5 ± 40.1 nmol/L vs. 11.3 ± 2.5 nmol/L; $P < 0.05$) were significantly elevated in patients compared to controls (Fig. 3C). The presence of excessive DoxSBs and DoxCers also supports the pathogenicity of the N177D mutation. The highest DoxCer level was found in #0005 (Fig. 3C) who showed the most severe phenotype (CMTNS = 27).

qMRI evaluation

Sphingolipids are highly enriched in nerves. The N177D mutation is expected to damage both myelin and axon, which are in line with the nonuniform slowing of conduction velocities and the reduced amplitudes in NCS found in our patients as well as the previously reported cases. To further assess the nerve pathology, we imaged thigh muscles and sciatic nerves using qMRI in several patients with the N177D mutation.

Fat increases in denervated muscles; thus, muscle FF has been used as proxy to evaluate axonal loss indirectly. Whole muscle FF was significantly elevated ($P = 0.015$; Fig. 4C9) in patients with HSN1C (16.2 ± 1.7 ; Table 3) compared with controls (10.8 ± 2.8 ; Table 3), supporting axonal loss.

Distal nerves were nonresponsive in NCS. The “burn-out” tissues would not provide accurate information for ongoing nerve pathology. Instead, we targeted proximal nerves (sciatic) using qMRI. Multiparametric qMRI of the sciatic nerve was performed at mid-thigh level to measure the total area of nerve fascicles (fCSA) and to acquire quantitative maps of T1, PD, R2*, R2, MTR, ADC, and FA. T1 reflects the relaxation time of the longitudinal magnetization, whereas PD is the overall magnitude of the magnetization. R2 (R2*) is the relaxation rate of the (effective) transverse magnetization. MTR measures the signal suppression ratio by the magnetization transfer effect between the free water pool and bound water pool

(macromolecules). ADC and FA are indices reflecting water diffusion directions. In general, nerve tissues with higher intra/extra-cellular water content have higher in T1, PD, ADC, and lower in R2 (R2*). Demyelination may further decrease MTR and FA.

On the high-resolution T1-weighted image, sciatic nerve fascicles were hyperintense surrounded by hypointense fatty tissues (Fig. 4A1 and B1). Compared with controls, patients with HSN1C had severely hypertrophic fascicles, leading to an increase of fCSA (Table 3 and Fig. 4C1; 107.5 ± 61.9 in HSN1C vs. 17.1 ± 1.9 in controls; $P = 0.003$). One of the patients (#0003) had an fCSA 10 times larger than the mean of control fCSA. Hypertrophy appeared to be intra-fascicular. Spaces around fascicles (epi-/perineurium) were qualitatively unchanged (Fig. 4A1 and B1).

Moreover, we observed significantly increased T1 ($P < 0.001$; Fig. 4C2), PD ($P < 0.001$; Fig. 4C3) and ADC ($P < 0.001$; Fig. 4C7), and decreased MTR ($P = 0.001$; Fig. 4C6), R2* ($P < 0.001$; Fig. 4C4) and FA ($P = 0.010$; Fig. 4C8) values in patients. These findings suggest an increase in water content and decrease in myelin since MTR is sensitive to myelin content.

Discussion

HSN1C is an extremely rare disease, but its biological implications have drawn significant attentions for multiple reasons: (1) SPT is a key enzyme catalyzing sphingolipid synthesis. Sphingolipid is enriched in myelin and vital for nerve functions, including action potential propagation; (2) *SPTLC1* or *2* encodes a protein subunit essential to the SPT enzyme complex. Missense mutations in *SPTLC1* or *2* resulted in excessive DoxSLs that are neurotoxic.⁹ DoxSLs are also increased in patients with idiopathic axonal polyneuropathy and diabetic neuropathy,³¹ the disorder with the highest prevalence among all peripheral nerve diseases. Moreover, patients with

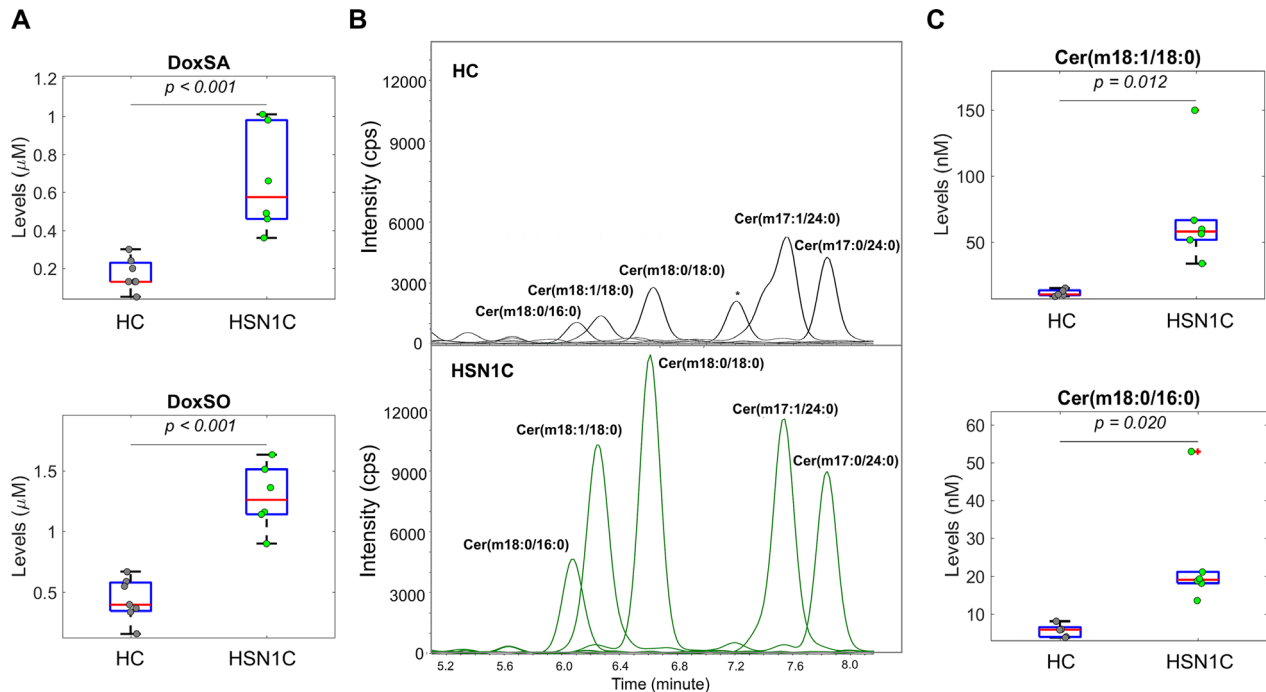


Figure 3. Quantification of plasma DoxSLs. (A) Two DoxSBs, Deoxy-sphinganine (DoxSA) and deoxy-sphingosine (DoxSO), in the plasma were significantly increased in six patients compared with seven healthy controls (HCs) ($P < 0.001$). (B) Extracted chromatogram of DoxCers was from a patient (#0005, green) and a control (#0008, black). X-axis is the retention times for individual DoxCers. Asterisk points to an unidentified isobar to Cer(m17:0/24:0) that was eluted earlier than the actual compound. (C) Comparison of two DoxCer concentrations was made between six patients and five HCs. Cer(m18:0/16:0) and Cer(m18:1/18:0) were significantly increased in patients ($P < 0.05$).

peripheral neuropathies due to mitochondrial disorders (PMD)³² or paclitaxel chemotherapy for cancer have been shown to have elevated DoxSLs in their plasma³³; (3) Although pending to be confirmed in controlled trials, elegant studies have shown that pathological changes in HSN1C may be blocked or even reversed using a modified diet with an altered level of amino acids,¹⁶ thereby offering promising therapeutic potential.

A recent study has shown that five patients with the N177D mutation co-segregated with HSN1C phenotype.³⁰ According to the ACMG-AMP variant classification guidelines and the latest update in ClinVar for this variant (in April 17, 2020), this variant has been classified as a Variant of Uncertain Significance (VUS) with conflicting interpretations of pathogenicity.³⁴ Our study adds another family with six patients showing co-segregation of the N177D mutation. Furthermore, both studies have demonstrated the increased DoxSLs in all 11 patients with the N177D mutation. Together, these findings collectively provide compelling evidence for the pathogenicity of N177D.

There were two additional variants (T44S in *PMP22* and R725H in *SCN11A*) identified in this family. One might question whether T44S and R725H have modified the phenotype. This is unlikely. For instance, #0006 had all three mutations, but developed a very mild phenotype

with a CMTNS of 4 at 63 years of age. In contrast, a 33-year-old #0003 with two mutations (T44S and N177D) had a sciatic nerve size 10 times greater than that of controls (178.9 vs. 17.1 mm²; Fig. 4) and a CMTNS of 24.

Our NCS showed that the conduction velocities (CV) were nonuniform in this family, which is typically seen in patients with acquired demyelinating polyneuropathies such as Guillain-Barré Syndrome (GBS), chronic inflammatory demyelinating polyneuropathy (CIDP) as well as a few inherited peripheral nerve diseases including CMTX1³⁵ and CMT4J.²⁷ A similar pattern of CV was also observed in another family with the N177D mutation.³⁰ We therefore reviewed all 13 HSN1 studies with NCS data (summarized in Table 4). Only two of these 13 studies provided CVs from paired nerves in the same limbs (median vs. ulnar or peroneal vs. tibial). They all showed nonuniform slowing of CVs.^{2,4} Another five studies showed CVs in unpaired nerves that ranged from ~20s to ~60s m/sec, which is also suggestive of segmental demyelination.^{1,36–39} Moreover, pathological segmental demyelination has been shown in a postmortem examination of a HSN1 patient.² In addition, leg nerves were often nonresponsive, suggesting secondary axonal loss in large nerve fibers. The axonal loss in these patients is also supported by the increase in muscle FF values (Fig. 4C9). One study in patients with

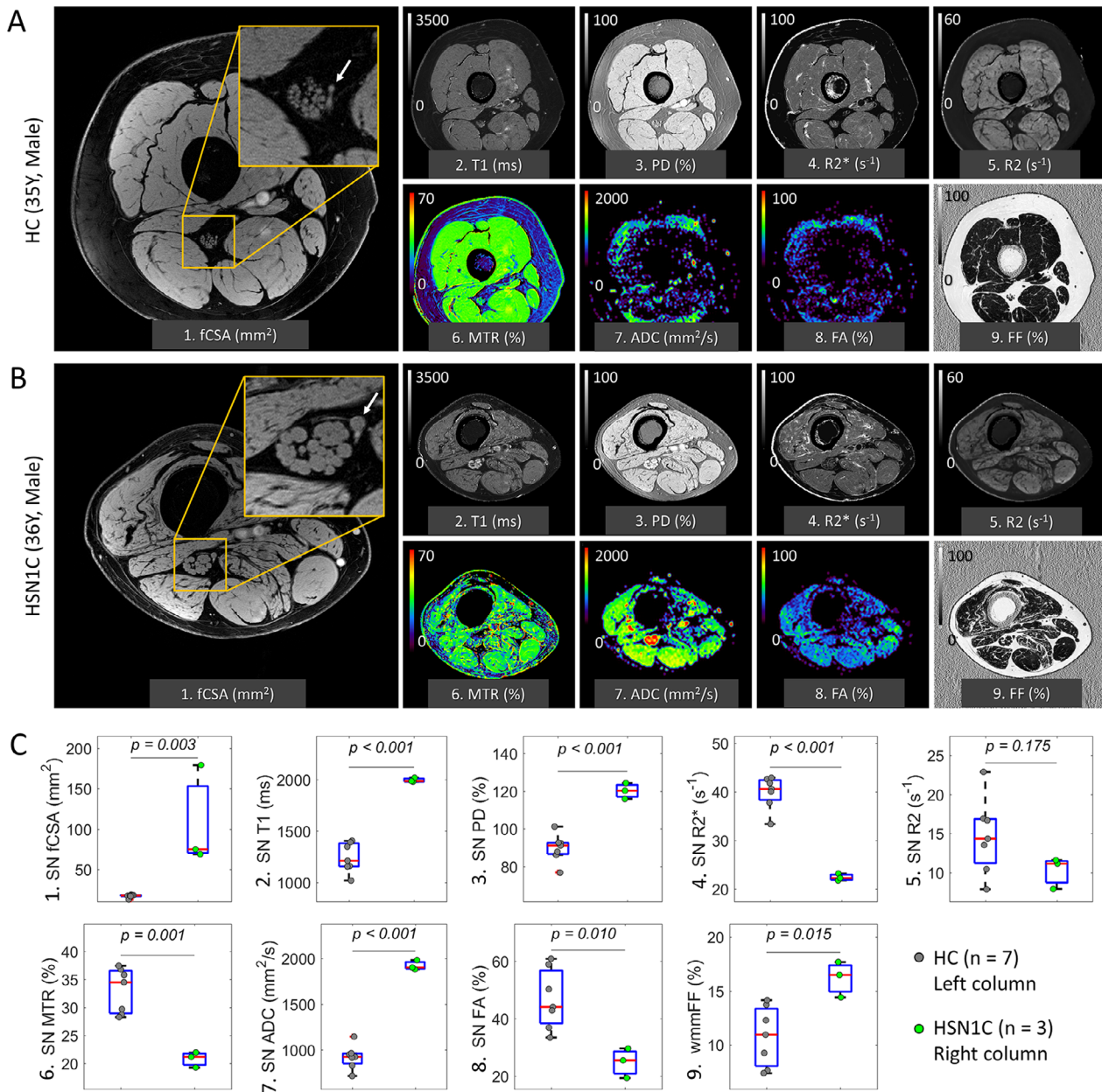


Figure 4. Quantitative magnetic resonance imaging (qMRI) study in muscle and sciatic nerve. Images in panel A and B are representative qMRI images from a HC (35-year-old, man) and a patient with HSN1C (36-year-old man, #0005). The fCSA measure and nerve fascicle mask were acquired with a resolution of $0.15 \times 0.15 \times 3.0$ mm³. Note that epineurium blood vessels (arrows on A1 and B1) were identified by their orientation and tracing adjacent slices. These vessels were excluded from nerve quantification. Resolutions for other images were as follows: $0.3 \times 0.3 \times 3.0$ mm³ for T1, PD and R2*; $0.6 \times 0.6 \times 3.0$ mm³ for R2 and MTR; $1.2 \times 1.2 \times 3.0$ mm³ for ADC and FA. The high-resolution GRE (A1 and B1), MTR (A6 and B6), and DTI (A7, A8, B7, and B8) scans were acquired using water excitation for suppressing fatty tissues, but not on other scans. Panel C plots the results of statistical analysis for muscle FF (C9) and sciatic nerve qMRI indices (C1 to C8). Gray scatters were data from controls; and green scatters were from patients. All these nerve qMRI indices were statistically significant except for the R2. The PD data (C3) were the PD ratio between nerve and adjacent normal-appearing muscle region since PD map has scale differences across subjects.

C133Y, C133W, and V144D in *SPTLC1* found no evidence of autonomic involvement,³⁷ supporting the term HSN1, not HSN1C. Together, these observations argue strongly that mutations in *SPTLC1* or 2 cause a demyelinating

polyneuropathy with secondary axonal loss. While small fibers (nonmyelinated) are involved in the disease, autonomic dysfunction is not a prominent feature in the disease.

Table 3. Demographics and data in qMRI.

	HC (n = 7)	HSN1C (n = 3)	P-value
Age (years)	30.1 ± 4.1 (26.0–38.0)	31.3 ± 5.0 (26.0–36.0)	0.704
BMI (kg/m ²)	23.8 ± 2.4 (19.2–26.2)	21.6 ± 0.4 (21.3–22.0)	0.163
Muscle – wmmFF (%)	10.8 ± 2.8 (7.4–14.1)	16.2 ± 1.7 (14.4–17.7)	0.015*
Nerve – fCSA (mm ²)	17.1 ± 1.9 (12.9–18.8)	107.5 ± 61.9 (68.8–178.9)	0.003*
Nerve – MTR (%)	33.0 ± 4.0 (28.3–37.5)	20.8 ± 1.4 (19.2–21.9)	0.001*
Nerve - T1 (ms)	1242 ± 144 (1020–1406)	1994 ± 21 (1979–2017)	<0.001*
Nerve – PD (%)	89.8 ± 7.4 (76.8–101.2)	120.2 ± 4.2 (115.9–124.3)	<0.001*
Nerve - R2* (s ⁻¹)	39.8 ± 3.4 (33.3–42.8)	22.4 ± 0.7 (21.7–23.1)	<0.001*
Nerve - R2 (s ⁻¹)	14.7 ± 4.9 (7.9–22.9)	10.2 ± 2.0 (7.9–11.6)	0.175
Nerve - ADC (mm ² /s)	921 ± 132 (715–1146)	1922 ± 53 (1882–1983)	<0.001*
Nerve - FA (%)	46.8 ± 10.5 (33.4–60.9)	24.8 ± 5.2 (19.3–29.6)	0.010*

Data were presented as mean ± standard deviation (range).

HC, Healthy control; BMI, Body mass index; wmmFF, whole-muscle mean fat fraction; fCSA, fascicular cross-sectional area; MTR, magnetization transfer ratio; T1, longitudinal relaxation time; PD, Proton density; R2*, Effective transverse relaxation rate; R2, transverse relaxation rate; ADC, Apparent diffusion coefficient; FA, Fractional anisotropy.

*Statistically significant.

Table 4. Key features in published families.

Reference	Dx (Genetic mutation)	DoxSLs	CV (m/s)	Nerve biopsy pathology
Suriyanarayanan et al. ³⁰	HSAN1C (SPTLC2, N177D)	Y	10–37	NA
Boso et al. ³⁶	HSAN1 (SPTLC1, C133F)	Y ¹	22–46	Almost complete loss of myelinated fibers
Ferreira et al. ³²	Neuropathy with mitochondrial disorders	Y ¹	NA	NA
Hube et al. ³¹	Idiopathic axonal polyneuropathy	Y	33 ± 21	Increased inflammation
Suriyanarayanan et al. ³	HSAN1C (SPTLC2, R183W)	Y	38 to normal	Severe loss of myelinated fibers
Kramer et al. ³³	Paclitaxel-induced neuropathy	Y ¹	NA	NA
Ernst et al. ³⁸	HSAN1C (SPTLC2, S384F)	Y	28–56	NA
Fridman et al. ¹	HSAN1 (SPTLC1, C133Y, and C133W)	NA	30–58	NA
Murphy et al. ³⁹	HSAN1 (SPTLC2, A182P)	Y	25–33	NA
Houlden et al. ²	HSAN1 (SPTLC1, C133W)	NA	18–58	Loss of myelinated axons and segmental demyelination
Geraldes et al. ³⁷	HSAN1 (SPTLC1, C133Y, C133W, and V144D)	NA	25–63	NA

Dx, Diagnosis; DoxSLs, Deoxy-sphingolipids; CV, Conduction Velocity; NA, Not Available; NR, Nonresponsive.

¹Marks studies with additional species of DoxCers analyzed.

The NCS findings raise the question if there are inflammatory activities in patients with HSN1. This question may not be well addressed by sural nerve biopsy. There were many HSN1 patients who had undetectable sensory nerve action potential (SNAP) in their legs. Sural nerves may be depleted of myelinated nerve fibers³ which is replaced by proliferated interstitial cells and collagen fibers. If there were any inflammatory cells, it would not be shown in the “burn out” nerve biopsies. Since genetic tests have become available, sural nerve biopsy is no longer justifiable for diagnosis.

Instead, we explored this issue by targeting on the proximal nerve (sciatic) using our recently developed peripheral nerve qMRI methods modified from the STAGE technique established by our MRI team.²² A

proximal nerve would have more myelinated nerve fibers preserved due to the fact that length-dependent degeneration affects the distal nerves first. However, the proximal nerve cannot be accessed by the NCS technique. Moreover, the STAGE technique allowed us to acquire six MRI-sequences of both muscle and nerve within a reasonable time frame. HSN1 nerves were significantly increased in T1, PD, and ADC, but decreased in MTR, R2*, and FA values (Fig. 4). Interestingly, a similar MRI pattern has been found in peripheral nerves in patients with CIDP²² and multiple sclerosis lesions in the brain.⁴⁰ CIDP also showed hypertrophic nerves.²² Moreover, sphingolipid metabolites have been suggested to contribute to the pathogenicity of neuro-inflammatory disorders including multiple sclerosis.⁸ Therefore, it is reasonable to

speculate an active inflammatory process in HSN1 proximal nerves. Proximal nerves in live patients are not accessible for pathological confirmation. It would also be difficult to recapitulate the combination of the chronicity of human HSN1 nerve and inflammatory activities in transgenic animal models with an overexpression of mutant protein.^{14–16} Thus, MRI in proximal nerves is helpful in this regard.

Our study identified diverse species of DoxCers in patients with the N177D mutation. This may help broaden our understanding of DoxSLs in the pathogenesis of the disease. So far, DoxSBs have been shown to be increased in patients with HSN1C^{9,30} and other types of neuropathies, but only a few studies have explored additional species of DoxCers in the patients (Table 4). It is generally known that these metabolites may affect the integrity of the cell membrane and thereby change cellular structure and function.⁵ However, different DoxSL species may have diverse biological effects⁵ that may contribute to variable phenotypic features in patients.^{16,17} Also, it has been shown that distinct species of DoxSLs are increased in HSN1 patients with a different SPT mutation.^{4,9} Elevation of both DoxCers and DoxmethCers in patients' plasma suggests a change in SPT specificity toward L-alanine and glycine. Whether these DoxSL subtypes can affect clinical variability in these patients requires further investigations. Therefore, sphingolipidome approach in HSN1 may offer different perspective into the pathogenesis of the neuropathies. Ongoing efforts in our laboratory are being undertaken to expand this study to a large cohort of patients.

In summary, our data support a demyelinating polyneuropathy in patients with HSN1C caused by the N177D mutation in *SPTLC2*. Our peripheral nerve qMRI data led us to speculate an active inflammatory process in the disease; and emphasizes importance for studying proximal nerves in chronic peripheral nerve diseases when distal nerves are degenerated. Our results are also relevant to clinical practice. Along with CMTX1 and CMT4J, this study adds another inherited peripheral nerve disease (HSN1) into the list that may resemble the electrophysiological phenotype of CIDP with nonuniform slowing of conduction velocity. This would be particularly problematic in differential diagnosis when dealing with patients with de novo mutations or absence of family history. On the other hand, these monogenic demyelinating polyneuropathies demand explanations how genetic background predisposes humans to develop “acquired” demyelination diseases like CIDP.

Conflict of Interest

The authors do not have any conflict of interest.

References

1. Fridman V, Oaklander AL, David WS, et al. Natural history and biomarkers in hereditary sensory neuropathy type 1. *Muscle Nerve* 2015;51:489–495.
2. Houlden H, King R, Blake J, et al. Clinical, pathological and genetic characterization of hereditary sensory and autonomic neuropathy type 1 (HSAN I). *Brain* 2006;129:411–425.
3. Suriyanarayanan S, Auranen M, Toppila J, et al. The variant p. (Arg183Trp) in *SPTLC2* causes late-onset hereditary sensory neuropathy. *NeuroMol Med* 2016;18:81–90.
4. Roththier A, Auer-Grumbach M, Janssens K, et al. Mutations in the *SPTLC2* subunit of serine palmitoyltransferase cause hereditary sensory and autonomic neuropathy type I. *Am J Hum Genet* 2010;87:513–522.
5. Jiménez-Rojo N, Sot J, Busto Jon V, et al. Biophysical Properties of Novel 1-Deoxy-(dihydro)ceramides occurring in mammalian cells. *Biophys J* 2014;107:2850–2859.
6. Haribowo AG, Hannich JT, Michel AH, et al. Cytotoxicity of 1-deoxysphingolipid unraveled by genome-wide genetic screens and lipidomics in *Saccharomyces cerevisiae*. *Mol Biol Cell* 2019;30:2814–2826.
7. Pujol-Lereis LM. Alteration of sphingolipids in biofluids: implications for neurodegenerative diseases. *Int J Mol Sci* 2019;20:3564.
8. Maceyka M, Spiegel S. Sphingolipid metabolites in inflammatory disease. *Nature* 2014;510:58–67.
9. Penno A, Reilly MM, Houlden H, et al. Hereditary sensory neuropathy type 1 is caused by the accumulation of two neurotoxic sphingolipids. *J Biol Chem* 2010;285:11178–11187.
10. Hojjati MR, Li Z, Jiang X-C. Serine palmitoyl-CoA transferase (SPT) deficiency and sphingolipid levels in mice. *Biochim Biophys Acta (BBA)* 2005;1737:44–51.
11. Gable K, Han G, Monaghan E, et al. Mutations in the yeast *LCB1* and *LCB2* genes, including those corresponding to the hereditary sensory neuropathy type I mutations, dominantly inactivate serine palmitoyltransferase. *J Biol Chem* 2002;277:10194–10200.
12. McCampbell A, Truong D, Broom DC, et al. Mutant *SPTLC1* dominantly inhibits serine palmitoyltransferase activity in vivo and confers an age-dependent neuropathy. *Hum Mol Genet* 2005;14:3507–3521.
13. Eichler FS, Hornemann T, McCampbell A, et al. Overexpression of the wild-type *SPT1* subunit lowers desoxysphingolipid levels and rescues the phenotype of HSN1. *J Neurosci* 2009;29:14646–14651.
14. Oswald MC, West RJ, Lloyd-Evans E, Sweeney ST. Identification of dietary alanine toxicity and trafficking dysfunction in a *Drosophila* model of hereditary sensory

- and autonomic neuropathy type 1. *Hum Mol Genet* 2015;24:6899–6909.
15. Cui M, Ying R, Jiang X, et al. A model of hereditary sensory and autonomic neuropathy type 1 reveals a role of glycosphingolipids in neuronal polarity. *J Neurosci* 2019;39:5816–5834.
 16. Garofalo K, Penno A, Schmidt BP, et al. Oral L-serine supplementation reduces production of neurotoxic deoxysphingolipids in mice and humans with hereditary sensory autonomic neuropathy type 1. *J Clin Invest* 2011;121:4735–4745.
 17. Othman A, Bianchi R, Alecu I, et al. Lowering plasma 1-deoxysphingolipids improves neuropathy in diabetic rats. *Diabetes* 2015;64:1035–1045.
 18. Murphy SM, Herrmann DN, McDermott MP, et al. Reliability of the CMT neuropathy score (second version) in Charcot-Marie-Tooth disease. *J Peripher Nerv Syst* 2011;16:191–198.
 19. Li J, Krajewski K, Shy ME, Lewis RA. Hereditary neuropathy with liability to pressure palsy. *Neurology* 2002;58:1769–1773.
 20. Bielawski J, Szulc ZM, Hannun YA, Bielawska A. Simultaneous quantitative analysis of bioactive sphingolipids by high-performance liquid chromatography-tandem mass spectrometry. *Methods* 2006;39:82–91.
 21. Gaver RC, Sweeley C. Methods for methanolysis of sphingolipids and direct determination of long-chain bases by gas chromatography. *J Am Oil Chem Soc* 1965;42:294–298.
 22. Chen Y, Haacke EM, Li J. Peripheral nerve magnetic resonance imaging. *F1000Res* 2019;8:1803. <https://doi.org/10.12688/f1000research.9695.1>
 23. Chen Y, Liu S, Buch S, et al. An interleaved sequence for simultaneous magnetic resonance angiography (MRA), susceptibility weighted imaging (SWI) and quantitative susceptibility mapping (QSM). *Magn Reson Imaging* 2018;47:1–6.
 24. Zhang T, Chen Y, Bao S, et al. Resolving phase ambiguity in dual-echo Dixon imaging using a projected power method. *Magn Reson Med* 2017;77:2066–2076.
 25. Chen Y, Liu S, Wang Y, et al. Strategically Acquired Gradient Echo (STAGE) imaging, part I: creating enhanced T1 contrast and standardized susceptibility weighted imaging and quantitative susceptibility mapping. *Magn Reson Imaging* 2018;46:130–139.
 26. Stanisiz GJ, Odrobina EE, Pun J, et al. T1, T2 relaxation and magnetization transfer in tissue at 3T. *Magn Reson Med* 2005;54:507–512.
 27. Hu B, McCollum M, Ravi V, et al. Myelin abnormality in Charcot-Marie-Tooth type 4J recapitulates features of acquired demyelination. *Ann Neurol* 2018;83:756–770.
 28. Li J. Molecular regulators of nerve conduction—lessons from inherited neuropathies and rodent genetic models. *Exp Neurol* 2015;267:209–218.
 29. Saghira C, Bis DM, Stanek D, et al. Variant pathogenicity evaluation in the community-driven Inherited Neuropathy Variant Browser. *Hum Mutat* 2018;39:635–642.
 30. Suriyanarayanan S, Othman A, Dräger B, et al. A novel variant (Asn177Asp) in SPTLC2 causing hereditary sensory autonomic neuropathy type 1C. *NeuroMol Med* 2019;21:182–191.
 31. Hube L, Dohrn MF, Karsai G, et al. Metabolic syndrome, neurotoxic 1-deoxysphingolipids and nervous tissue inflammation in chronic idiopathic axonal polyneuropathy (CIAP). *PloS One* 2017;12:e0170583.
 32. Ferreira CR, Goorden SMI, Soldatos A, et al. Deoxysphingolipid precursors indicate abnormal sphingolipid metabolism in individuals with primary and secondary disturbances of serine availability. *Mol Genet Metab* 2018;124:204–209.
 33. Kramer R, Bielawski J, Kistner-Griffin E, et al. Neurotoxic 1-deoxysphingolipids and paclitaxel-induced peripheral neuropathy. *FASEB J* 2015;29:4461–4472.
 34. Nykamp K, Anderson M, Powers M, et al. Sherlock: a comprehensive refinement of the ACMG–AMP variant classification criteria. *Genet Med* 2017;19:1105.
 35. Gutierrez A, England JD, Sumner AJ, et al. Unusual electrophysiological findings in X-linked dominant Charcot-Marie-Tooth disease. *Muscle Nerve* 2000;23:182–188.
 36. Boso F, Armirotti A, Taioli F, et al. Deoxysphingolipids as candidate biomarkers for a novel SPTLC1 mutation associated with HSAN-I. *Neurol Genet* 2019;5:e365.
 37. Geraldine R, De Carvalho M, Santos-Bento M, Nicholson G. Hereditary sensory neuropathy type 1 in a Portuguese family—electrodiagnostic and autonomic nervous system studies. *J Neurol Sci* 2004;227:35–38.
 38. Ernst D, Murphy SM, Sathiyandan K, et al. Novel HSAN1 mutation in serine palmitoyltransferase resides at a putative phosphorylation site that is involved in regulating substrate specificity. *NeuroMol Med* 2015;17:47–57.
 39. Murphy SM, Ernst D, Wei Y, et al. Hereditary sensory and autonomic neuropathy type 1 (HSANI) caused by a novel mutation in SPTLC2. *Neurology* 2013;80:2106–2111.
 40. Blystad I, Håkansson I, Tisel A, et al. Quantitative MRI for analysis of active multiple sclerosis lesions without gadolinium-based contrast agent. *Am J Neuroradiol* 2016;37:94–100.